Geofísica Internacional (1998), Vol. 37, Num. 4, pp. 309-325

The dynamics of elongated and strongly stratified straits

S.N. Bulgakov and A. Martínez Zatarain
Instituto de Astronomía y Meteorología,
Universidad de Guadalajara, Jalisco, México.

Received: March 3, 1997; accepted: August 11, 1998.

RESUMEN

Un modelo tridimensional friccional de tipo Ekman fue derivado a partir del análisis de las ecuaciones de momento primitivo para casos de estrechos largos con una marcada estratificación. Obtuvimos una solución analítica. Se realizó una serie de experimentos de modelación destinados a investigar la formación de los patrones de circulación integral y la estructura tridimensional de la corriente como funciones del forzamiento externo y de los valores de parámetros en un canal de profundidad no uniforme rotante en el ß-plano. Se comparan los resultados de la modelación con datos hidrológicos observados en el estrecho de Bósforo.

PALABRAS CLAVE: dinámica de estrechos, modelo friccional.

ABSTRACT

A three-dimensional frictional Ekman-type model has been derived from an analysis of the primitive momentum equations for the cases of long, strongly stratified straits. An analytical solution has been obtained. A set of model experiments is developed to investigate the formation of depth-integrated circulation patterns and three-dimensional current structures, as functions of external forcing, and parameter values for channels having nonuniform depth, and rotating in the ß-plane. The model results are compared with hydrological data obtained for the Bosphorus strait.

KEY WORDS: Straits dynamics, frictional model.

INTRODUCTION

A strait is a constriction separating sea basins of different densities. There are numerous publications devoted to theoretical and experimental investigations of straits (Kinder and Burns, 1986), with particular interest in the influence of strait flows on the circulation of adjoining seas (Candela, 1991). Salinity exchange through the straits, coupled with river discharge, is likely to be an important driving force responsible for large-scale circulation in inland seas (Bulgakov *et al*., 1996a,b; Bulgakov and Kushnir, 1996).

The behavior of straits depends on their length, width, depth, and stratification. We describe circulation in long stratified straits, which differ more strongly from ordinary sea basins, and we investigate dynamics in such water bodies using mathematical modelling.

ANALYSIS OF MOMENTUM EQUATIONS

Consider the equation of motion for the longitudinal component of the velocity vector

$$\frac{\partial u}{\partial t} + u\frac{\partial u}{\partial x} + v\frac{\partial u}{\partial y} + w\frac{\partial u}{\partial z} - fu = -\frac{1}{\rho_0}\frac{\partial p}{\partial x} + A_l \Delta u + A_z \frac{\partial^2 u}{\partial z^2}, \quad (1)$$

where the axes *x,y,z* are directed along-strait, cross-strait and vertically downwards respectively.

Omitting the non-stationary term, we consider times T very much longer than the characteristic time-scale of long internal waves $T >> \frac{L}{(g' h)^{1/2}}$. Here L is the length of the strait, $g' = g\frac{\rho_2 - \rho_1}{\rho_2}$ is the reduced gravity, ρ_1 and ρ_2 are the density values of the upper and lower layers, and h is an interface depth.

To evaluate the other terms in equation (1) we define a turbulent friction law $\tau_b = cu^2$, where $c = O(10^{-3})$ is the drag coefficient. This relation may be justified on both theoretical and empirical grounds (Anati *et al*., 1977; Skiba, 1989). The parameter

$$\gamma_1 = c\frac{L}{H} \quad (2)$$

defines the ratio of turbulent bottom friction to nonlinear acceleration, where H is the depth of the strait. So equation (2) defines a short strait as one where $\gamma_1 << 1$; otherwise the strait will be defined as long.

For short straits, the influence of bottom friction may be neglected compared with the nonlinear terms. Then nonlinear acceleration balances the horizontal pressure gradient (Armi, 1986):

$$u\frac{\partial u}{\partial x} = -\frac{1}{\rho_0}\frac{\partial p}{\partial x} \quad . \tag{3}$$

If the flow is hydrostatic, and there is no net barotropic flow, the main equation of hydraulic control theory may be written as:

$$F^2 = \frac{u^2}{g' h} \quad . \tag{4}$$

The Froud number F is widely used in studies of short strait dynamics (Bryden and Kinder, 1991).

The counterpart of equation (4) for the case of a two-layered water approximation is

$$F^2 = \frac{u_1^2}{g' h_1} + \frac{u_2^2}{g' h_2} \quad . \tag{4'}$$

When F=1, the flow velocity equals the speed of long internal waves $U=(g'\cdot h)^{1/2}$. Such a hydraulic regime controls the flow. It is assumed (Armi and Farmer, 1985) that such control typically occurs in the strait's constriction, and in vicinity of the sills. On the other hand, for an elongated strait it is possible to neglect nonlinear acceleration in comparison with the vertical turbulent exchange term.

We consider the strait to be narrow if the square of the ratio of the horizontal scales

$$\gamma_2 = \left(\frac{D}{L}\right)^2 \tag{5}$$

is much less than unity, where D is the average width of the basin. It follows that in such straits $\frac{\partial^2}{\partial x^2} << \frac{\partial^2}{\partial y^2}$.

Now, if the boundary layer thickness does not exceed half the channel width $\pi\sqrt{\frac{2A_1}{f}} \le \frac{D}{2}$, we may obtain an upper limit for the coefficient of horizontal turbulent exchange $A_1 \le \frac{fD^2}{8\pi^2}$. The parameter

$$\gamma_3 = \frac{L}{8\pi^2 R} \tag{6}$$

defines the ratio of lateral exchange to horizontal pressure gradient, where $R = \frac{\sqrt{g' h}}{f}$ is the Rossby deformation radius. In the case of a strongly stratified strait γ_3<<1, the lateral exchange in the main force balance is insignificant (Bulgakov, 1993).

According to Ekman theory, the basin is assumed to be deep if the quantity

$$\gamma_4 = 2\alpha H \tag{7}$$

exceeds unity, where $\alpha = \sqrt{\frac{f}{2A_z}}$ is the Ekman parameter.

Thus, for a long, strongly stratified, deep water body we have the following formulation

$$A_z\frac{\partial^2 u}{\partial z^2} + fv = -g\frac{\partial \zeta}{\partial x} + g\int_0^z \frac{\partial \rho}{\partial x}dz, \tag{8}$$

$$A_z\frac{\partial^2 v}{\partial z^2} - fu = -g\frac{\partial \zeta}{\partial y} + g\int_0^z \frac{\partial \rho}{\partial y}dz, \tag{9}$$

$$\frac{\partial u}{\partial x} + \frac{\partial v}{\partial y} + \frac{\partial w}{\partial z} = 0 \tag{10}$$

with boundary conditions

$$z = 0: \ A_z\frac{\partial u}{\partial z} = -\tau_x, \ A_z\frac{\partial v}{\partial z} = -\tau_y, \ w = 0 \tag{11}$$

$$z = H: \ u = v = w = 0 \ . \tag{12}$$

This is a classical generalized Ekman problem for current modelling in a baroclinic ocean (Ekman, 1932). It enables us to determine the three-component velocity vector (u,v,w) for a given distribution of density gradients (ρ_x, ρ_y) and wind stresses (τ_x, τ_y). A method for the determination of the free surface (ζ), and the formulation of additional boundary conditions at the lateral boundaries will be proposed below.

COMPARATIVE CHARACTERISTICS OF THE STRAITS

The main features of five straits are presented in Table 1 (Assaf and Hecht, 1974; Supplement to Atlas of Seas and Oceans, 1980; Tolmazin, 1985; Maderich and Efroimson, 1990).

Table 1

Comparative characteristics of straits

Strait	L (km)	D (km)	H (m)	S_1 ($^0/_{00}$)	S_2 ($^0/_{00}$)	ψ_0 (km^3/y)	g' (m/s^2)	R (km)	γ_1	γ_2	γ_3	γ_4
Gibraltar	60	20	360	36.15	37.75	1520	0.012	14.7	1.0	0.1100	0.05	72
Bosphorus	30	1	50	19.00	37.00	180	0.131	18.1	3.6	0.0011	0.02	10
Dardanelles	60	4	70	23.00	39.00	180	0.117	20.2	5.1	0.0044	0.04	14
B/Mandeb	160	30	180	36.60	39.70	840	0.023	14.4	5.3	0.0350	0.14	36
Kerchensky	40	20	20	10.80	18.00	20	0.053	7.3	12.0	0.2500	0.07	4

The density field was calculated using the linear state equation

$$\rho = \rho_0 \cdot (1 + \beta_S \cdot S) \qquad (13)$$

where ρ_0=1 g/cm^3 and β_S=0.75·10^{-3} (Oguz *et al*., 1990). The Ekman parameter α is of order $O(10^{-3})$ cm^{-1} for usual values of A_z. In accordance with Maderich and Efroimson (1986, 1990) the drag coefficient is taken as c=6·10^{-3} which results in good agreement between the model and observed water exchange values through the Gibraltar and Bosphorus straits.

Note from Table 1 that the Bosphorus, the Dardanelles and Bab-el-Mandeb have large values of γ_1. These are examples of long straits. Since γ_3 is small, they are also strongly stratified. The Gibraltar strait is an intermediate strait with γ_1=1. The Kerchensky strait is shallow, since γ_4 approaches unity.

In this study, we consider the Bosphorus strait which is oriented in a north-south direction (Figure 1). Its coastline is fairly indented. The width varies from 0.7 to 3.5 km with an average value of 1.3 km at the surface, and 0.5 km at a depth of 50 m. The constriction is located nearly 10 km from the southern exit into the Marmara Sea, and it extends for nearly 2.5 km, whilst the depth varies between 30 m and 100 m. The bottom topography features two sills at the northern and southern ends of the strait (Unluata *et al*., 1990).

The salinity transect along the Bosphorus strait is shown in Figure 2, indicating a typical distribution in $S(x,z)$ (Unluata *et al*., 1990). The distinctive feature of this salinity distribution is presence of uniformly sloping isohalines along the major axis, although the behavior of the isohalines differs near the constriction and the southern sill. Theoretical (Wang, 1987) and laboratory (Anati *et al*., 1977) investigations suggest that the interface rises linearly in the upper flow direction.

The main features of the salinity distribution across the strait have not been discussed in the scientific literature, possibly because of the minute salinity differences between the lateral boundaries.

Observations and analyses of currents in the Bosphorus suggest a two-layered structure, where the upper current moves in a southerly direction, and the lower current is the reverse. The latter current is responsible for transferring saltier Marmara Sea waters to the Black Sea. The longitudinal flow velocity in both layers approaches a few tens of cm/s; some typical vertical profiles $u(z)$ (Merz, 1929) are represented in Figure 3. Transverse circulation is negligible, of order of a few cm/s.

One of the primary unresolved questions in the dynamics of this strait concerns its three-dimensional current structure. Currently, there exist only two-dimensional (Tolmazin, 1967; Johns and Oguz, 1990) and two-layered (Bogdanova and Stepanov, 1974; Maderich and Efroimson, 1990; Oguz *et al*., 1990) models of this waterway. Uncertainties also exist concerning the mechanism

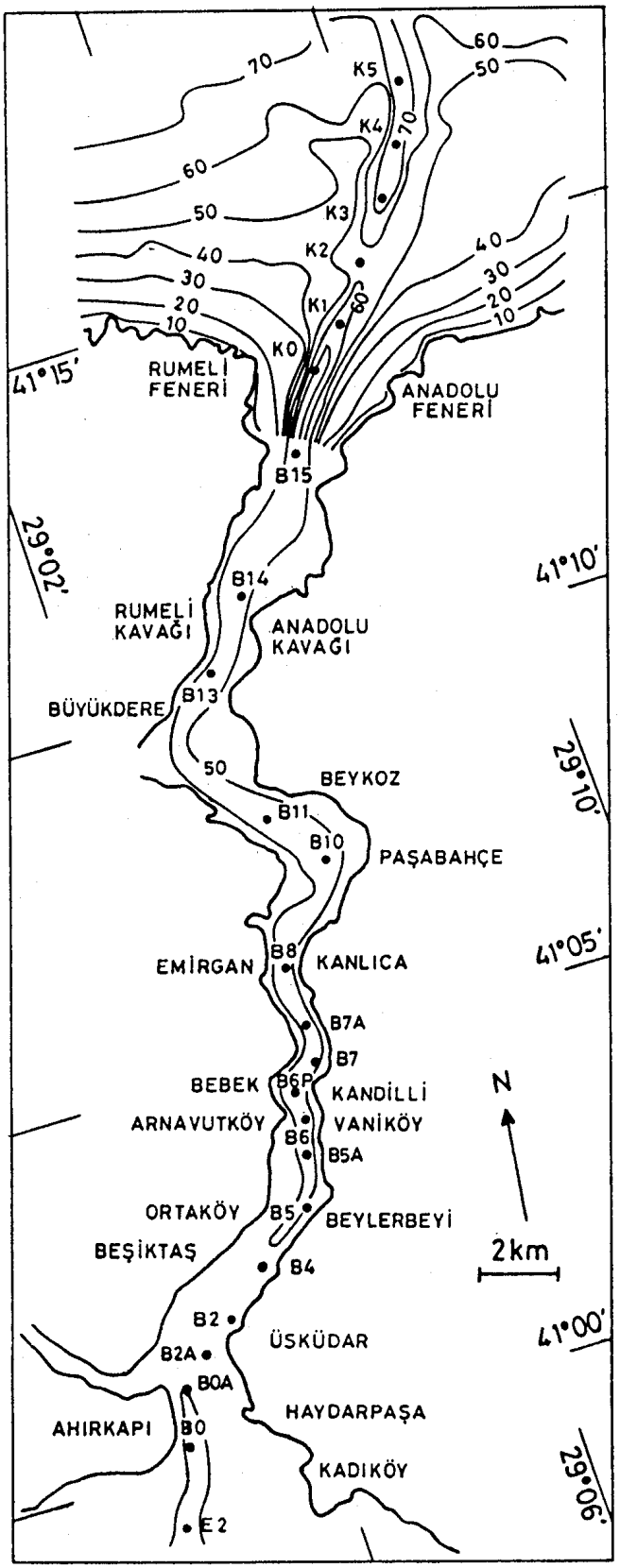

Fig. 1. Plan of the Bosphorus, together with the locations of the hydrographic stations. Adapted from Unluata *et al*., 1990.

responsible for creating the two-layered current system, and the influence of external factors on the vertical and horizontal circulation. Similarly, there is no generally accepted view of the blocking conditions of the Bosphorus undercurrent, or of the north-westward spreading of the Marmara Sea waters into the Black Sea (Figure 4).

THE STRAIT MODEL

We use equations (8)-(10) with boundary conditions (11)-(12) to describe three-dimensional water circulation in an idealized rectangular long channel, rotating in the β-plane, and with vertical lateral boundaries and a variable bottom topography. We assume that $H(x)$ is a known function along the main axis, and that there are asymmetrical sills at the ends of the strait. Axes x,y,z are directed to the north, west and vertically downwards, respectively, whilst the origin of the coordinates is at the eastern coast of the southern sill.

We assume a homogeneous wind force at the surface. The three-dimensional density field is defined by setting average slopes of equal density ρ_x and ρ_y along and across the strait. Observations across the Gibraltar strait (Kinder and Bryden, 1990) support this assumption (Figure 5).

The analytical solution of problem (8)-(12) is obtained by a Fourier method, assuming that the horizontal density gradients are constant. We represent the solution as a linear combination of the level slopes

$$u = -\frac{\partial \zeta}{\partial x} u_1(z) - \frac{\partial \zeta}{\partial y} u_2(z) + u_3(z) \qquad (14)$$

$$v = -\frac{\partial \zeta}{\partial x} v_1(z) - \frac{\partial \zeta}{\partial y} v_2(z) + v_3(z) \quad . \qquad (15)$$

Then the coefficients u_i, v_i (i=1,2,3) can be found from the three systems of equations

$$A_z \frac{\partial^2 u_1}{\partial z^2} + f v_1 = g, \quad z = 0 : \frac{\partial u_1}{\partial z} = \frac{\partial v_1}{\partial z} = 0, \qquad (16)$$

$$A_z \frac{\partial^2 v_1}{\partial z^2} - f u_1 = 0, \quad z = H : u_1 = v_1 = 0,$$

$$A_z \frac{\partial^2 u_2}{\partial z^2} + f v_2 = 0, \quad z = 0 : \frac{\partial u_2}{\partial z} = \frac{\partial v_2}{\partial z} = 0, \qquad (17)$$

$$A_z \frac{\partial^2 v_2}{\partial z^2} - f u_2 = g, \quad z = H : u_2 = v_2 = 0,$$

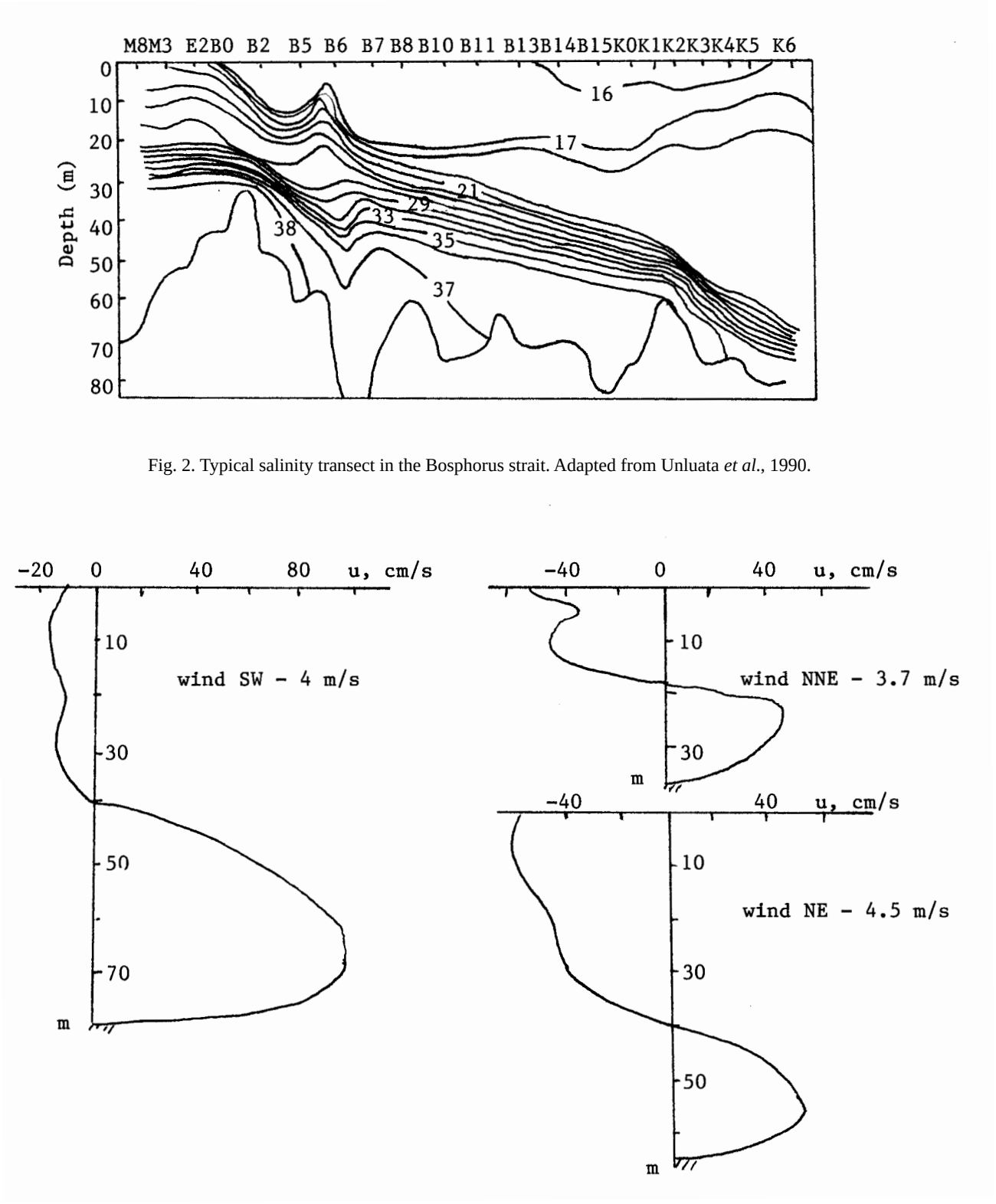

Fig. 2. Typical salinity transect in the Bosphorus strait. Adapted from Unluata *et al*., 1990.

Fig. 3. Current meter profiles *u*(z) based on instrumental data (Merz, 1929). Adapted from Tolmazin, 1967.

$$A_z \frac{\partial^2 u_3}{\partial z^2} + f v_3 = g\rho_x z, \quad z = 0 : A_z \frac{\partial u_3}{\partial z} = -\tau_x, A_z \frac{\partial v_3}{\partial z} = -\tau_y,$$

$$A_z \frac{\partial^2 v_3}{\partial z^2} - f u_3 = g\rho_y z, \quad z = H : u_3 = v_3 = 0. \qquad (18)$$

Using the complex velocity $U_k = u_k + i \cdot v_k$ (k = 1,2,3) and deep sea water approximation ($\gamma_4 >> 1$) we obtain the following analytical solutions for the velocity components, after separating real and imaginary parts:

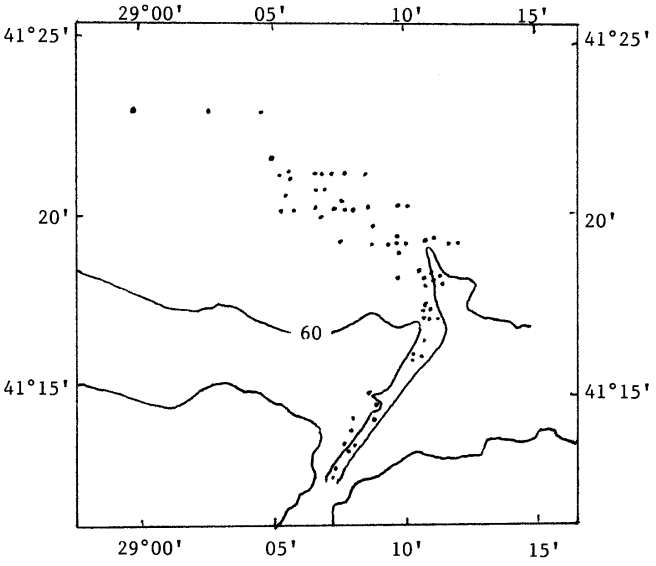

Fig. 4. Observed salinity distribution (>24‰) in a layer near the bottom of the Bosphorus strait, at the northern exit into the Black Sea. Adapted from Unluata *et al*., 1990.

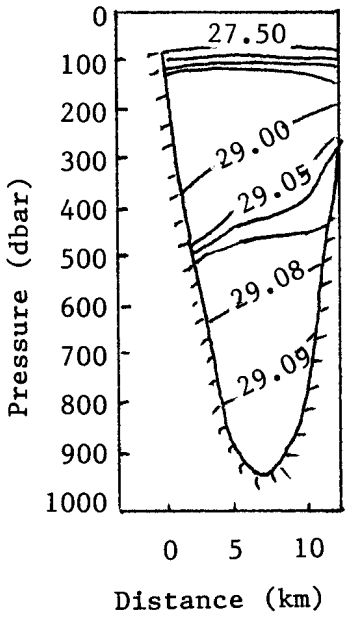

Fig. 5. Cross-strait section of potential density in the Gibraltar strait. Adapted from Kinder and Bryden, 1990.

$$u=\frac{g}{f}e^{-\alpha z}\left[\sin\alpha z\left(\frac{\rho_x+\rho_y}{2\alpha}-\alpha\frac{\tau_x-\tau_y}{g}\right)+\cos\alpha z\left(\frac{\rho_x-\rho_y}{2\alpha}+\alpha\frac{\tau_x+\tau_y}{g}\right)\right]+\frac{g}{f}e^{-\alpha(H-z)}\left[\sin\alpha(H-z)\left(\frac{\partial\zeta}{\partial x}-H\rho_x\right)-\cos\alpha(H-z)\left(\frac{\partial\zeta}{\partial y}-H\rho_y\right)\right]+\frac{g}{f}\left(\frac{\partial\zeta}{\partial y}-z\rho_y\right), \quad (19)$$

$$v=\frac{g}{f}e^{-\alpha z}\left[\cos\alpha z\left(\frac{\rho_x+\rho_y}{2\alpha}-\alpha\frac{\tau_x-\tau_y}{g}\right)-\sin\alpha z\left(\frac{\rho_x-\rho_y}{2\alpha}+\alpha\frac{\tau_x+\tau_y}{g}\right)\right]+\frac{g}{f}e^{-\alpha(H-z)}\left[\cos\alpha(H-z)\left(\frac{\partial\zeta}{\partial x}-H\rho_x\right)+\sin\alpha(H-z)\left(\frac{\partial\zeta}{\partial y}-H\rho_y\right)\right]-\frac{g}{f}\left(\frac{\partial\zeta}{\partial x}-z\rho_x\right), \quad (20)$$

$$w=\frac{g\beta}{f^2}\left[\begin{array}{l}(1-e^{-\alpha z}\cos\alpha z)\left(\frac{\rho_x}{\alpha^2}+\frac{\tau_y}{g}\right)-e^{-\alpha z}\sin\alpha z\left(\frac{\rho_y}{\alpha^2}-\frac{\tau_x}{g}\right)+z\left(\frac{\partial\zeta}{\partial y}-\frac{1}{2}z\rho_y\right)-\\ -\alpha z e^{-\alpha z}\cos\alpha z\left(\frac{\rho_x-\rho_y}{4\alpha^2}+\frac{\tau_x+\tau_y}{2g}\right)-\alpha z e^{-\alpha z}\sin\alpha z\left(\frac{\rho_x+\rho_y}{4\alpha^2}-\frac{\tau_x-\tau_y}{2g}\right)\end{array}\right]+$$

$$\frac{g}{2\alpha f}\left\{\begin{array}{l}e^{-\alpha(H-z)}\sin\alpha(H-z)\left[2\alpha H_x\left(\frac{\partial\zeta}{\partial x}+\frac{\partial\zeta}{\partial y}-H\rho_x-H\rho_y\right)+\frac{3\beta}{f}\left(\frac{\partial\zeta}{\partial y}-H\rho_y\right)\right]+\\ +\alpha(H-z)e^{-\alpha(H-z)}\sin\alpha(H-z)\frac{\beta}{f}\left(\frac{\partial\zeta}{\partial x}-H\rho_x\right)-\\ -\alpha(H-z)e^{-\alpha(H-z)}\cos\alpha(H-z)\frac{\beta}{f}\left(\frac{\partial\zeta}{\partial y}-H\rho_y\right)\end{array}\right\}. \quad (21)$$

These are the exact solutions of (8)-(10), and also the approximate solutions to the boundary conditions (11)-(12) since $e^{\alpha H} >> e^{-\alpha H}$.

The longitudinal and transverse level slopes $\frac{\partial\zeta}{\partial x}$ and $\frac{\partial\zeta}{\partial y}$, included in (19)-(21), can be found by integrating equations (19)-(20) vertically from surface to bottom, using the stream function $\frac{\partial\psi}{\partial x}=\int_0^H v\,dz$ and $\frac{\partial\psi}{\partial y}=-\int_0^H u\,dz$. Then

$$\frac{\partial \zeta}{\partial x} = -\frac{f}{gH}\frac{\partial \psi}{\partial x} - \frac{1}{2\alpha H}\frac{f}{gH}\frac{\partial \psi}{\partial y} + \frac{\alpha H - 1}{2\alpha H}\left(\underline{H\rho_x} - \frac{\rho_y}{2\alpha}\right) - \frac{\tau_x}{\underline{gH}} - \frac{1}{2\alpha H}\frac{\tau_y}{gH}, \quad (22)$$

$$\frac{\partial \zeta}{\partial y} = \frac{1}{2\alpha H}\frac{f}{gH}\frac{\partial \psi}{\partial x} - \frac{f}{\underline{gH}}\frac{\partial \psi}{\underline{\partial y}} + \frac{\alpha H - 1}{2\alpha H}\left(\underline{H\rho_y} - \frac{\rho_x}{2\alpha}\right) - \frac{\tau_y}{\underline{gH}} + \frac{1}{2\alpha H}\frac{\tau_x}{gH}. \quad (23)$$

Cross-differentiation of (22)-(23) and elimination of the free surface yields the following equation for the stream function $\psi(x,y)$ in the case of a narrow strait (γ_2<<1):

$$\frac{\partial^2 \psi}{\partial y^2} + 2\alpha H\left(\frac{H_x}{H} - \frac{\beta}{f}\right)\frac{\partial \psi}{\partial y} = F(x) \ , \quad (24)$$

where

$$F(x) = \frac{Hg}{2\alpha f}\left(\frac{\alpha H\beta}{2f} - \frac{\beta}{f} - \frac{H_x}{H}\right)\rho_x - \frac{H^2 g}{2f}\left(2\alpha H_x + \frac{\beta}{f}\right)\rho_y + 2\left(\frac{H_x}{H} + \frac{\beta}{4f}\right)\frac{\tau_x}{f} - 2\alpha H_x \frac{\tau_y}{f}. \quad (25)$$

Thus the solution of (24) is

$$\psi(x,y) = c_1(x) \bullet \exp\left[2\alpha H\left(\frac{\beta}{f} - \frac{H_x}{H}\right)y\right] + c_2(x) + \frac{fF}{2\alpha(fH_x - \beta H)}y, \quad (26)$$

where the constants $c_i(x)$ may be obtained from the boundary conditions at the lateral boundaries

$$y=0: \quad \psi=\psi_0, \quad y=D: \quad \psi=0 \ . \quad (27)$$

We now choose the parameter values. Consider a length $L=3\cdot10^6$ cm and a width $D=2\cdot10^5$ cm; we may define the bottom topography as

$$H(x) = \begin{cases} \left[7 - 3\left(2\frac{x}{L} - 1\right)^4\right]10^3 cm, 0 \le x \le \frac{L}{2} \\ \left[7 - 2\left(2\frac{x}{L} - 1\right)^4\right]10^3 cm, \frac{L}{2} \le x \le L \end{cases} \ , \quad (28)$$

with a maximum depth of 70 m, and two sills at depths of 50 m and 40 m at the northern and southern ends of the strait. We define the water exchange through the strait as $\psi_0 = -6\cdot10^9$ cm^3/s; a value which may be estimated in sea-strait systems from the water budget (river discharge and difference of evaporation and precipitation) in the adjoining sea.

We estimate the longitudinal density gradient as $\rho_x = -0.56\cdot10^{-9}$ cm^{-1}, which agrees with the observed horizontal salinity difference of 2‰ between the northern and southern boundaries of the Bosphorus strait. The cross-strait density slope $\rho_y = -0.24\cdot10^{-9}$ cm^{-1} is found from the dimensionless variables in equation (24), adopting the second item on the right side of eq. (25) as the main term. This corresponds to a salinity difference of 0.06‰ between the lateral boundaries of the strait. Finally, we assume g=10^3 cm/s^2, $\alpha=10^{-3}$ cm^{-1} and we define $f=f_0+\beta x$, where $f_0=10^{-4}$s^{-1} and $\beta=2\cdot10^{-13}$ cm^{-1}s^{-1}.

By using equations (19)-(20) describing the horizontal circulation, we may ensure that the solutions include the geostrophic balance, and the Ekman layer contributions (first two terms in square brackets). The geostrophic balance equations consist of the barotropic component caused by the surface level slope which does not vary with depth, and the baroclinic term which arises from the horizontal density gradient, and which does vary with depth.

Now, it is clear that a two-layer current system must be formed in such a strait. Thus, without the transverse level slope $\frac{\partial \zeta}{\partial y}$, the geostrophic velocity for the longitudinal current component varies from zero at the surface to a positive value ($-gH\rho_y/f$) of the order of tens of cm/s at the bottom. From the terms in equation (23) (where the main terms are underlined) it follows that for weak and moderate wind velocities, the cross-strait level slope becomes negative but not less than $-|H\rho_y|$. Therefore, the vertical current profile is shifted from the positive region by a negative term $\frac{g}{f}\frac{\partial \zeta}{\partial y}$, and two opposing layered currents are formed.

Lower current blocking is possible in the case of extremely strong easterly winds ($\tau_y \cong 10$) when the following condition occurs:

$$\frac{\partial \zeta}{\partial y} \le H\rho_y \ . \quad (29)$$

The effect of possible variations in the density field is beyond the scope of the present investigation.

Condition (29) differs from the one previously obtained by Bulgakov (1991), since his analysis did not take account of the cross-strait density slope. Our conclusion does not support the view of Oguz and Rozman (1991), that only northerly winds create favourable conditions for the blocking of the Bosphorus undercurrent entering the Black Sea.

RESULTS OF THE MODEL EXPERIMENTS

The experiments listed in Table 2 were aimed at studying stream function features, and three-dimensional current structure in the strait as a function of external forcing (density field, wind stress, fresh water budget) and various physical parameters (coefficient of vertical turbulent exchange, β-effect, bottom topography).

Table 2

Experiments and parameter values (GCS)

Par. / Exp.	ρ_x (cm^{-1})	ρ_y (cm^{-1})	τ_x (cm^2/s^2)	τ_y (cm^2/s^2)	ψ (cm^3/s)	H (cm)	β ($cm^{-1}\cdot s^{-1}$)	α (cm^{-1})
1	0	0	0	0	$-6\cdot10^9$	$H(x)$	$2\cdot10^{-13}$	10^{-3}
2	$-0.56\cdot10^{-9}$	0	0	0	$-6\cdot10^9$	$H(x)$	$2\cdot10^{-13}$	10^{-3}
3	$-0.56\cdot10^{-9}$	$-0.24\cdot10^{-9}$	0	0	$-6\cdot10^9$	$H(x)$	$2\cdot10^{-13}$	10^{-3}
4	$-0.56\cdot10^{-9}$	-10^{-9}	0	0	$-6\cdot10^9$	$H(x)$	$2\cdot10^{-13}$	10^{-3}
5	$-0.56\cdot10^{-9}$	-10^{-9}	0	0	$-6\cdot10^9$	$7\cdot10^3$	$2\cdot10^{-13}$	10^{-3}
6	$-0.56\cdot10^{-9}$	-10^{-9}	0	0	$-6\cdot10^9$	$H(x)$	0	10^{-3}
7	$-0.56\cdot10^{-9}$	-10^{-9}	0	0	$-6\cdot10^9$	$H(x)$	$2\cdot10^{-13}$	$0.7\cdot10^{-3}$
8	$-0.56\cdot10^{-9}$	-10^{-9}	0	0	$-6\cdot10^9$	$H(x)$	$2\cdot10^{-13}$	$\pi\cdot10^{-3}$
9	$-0.56\cdot10^{-9}$	-10^{-9}	0	0	0	$H(x)$	$2\cdot10^{-13}$	10^{-3}
10	0	0	-1.0	0	0	$H(x)$	$2\cdot10^{-13}$	10^{-3}
11	$-0.56\cdot10^{-9}$	-10^{-9}	6.5	0	$-6\cdot10^9$	$H(x)$	$2\cdot10^{-13}$	10^{-3}
12	$-0.56\cdot10^{-9}$	-10^{-9}	-6.5	0	$-6\cdot10^9$	$H(x)$	$2\cdot10^{-13}$	10^{-3}
13	$-0.56\cdot10^{-9}$	-10^{-9}	0	6.5	$-6\cdot10^9$	$H(x)$	$2\cdot10^{-13}$	10^{-3}
14	$-0.56\cdot10^{-9}$	-10^{-9}	0	-6.5	$-6\cdot10^9$	$H(x)$	$2\cdot10^{-13}$	10^{-3}

In the first experiment (Figure 6), the density field was assumed to be homogeneous, and the contribution of the wind was taken to be negligible. The only driving force arises from the positive water budget in the adjoining sea. The peak values of the stream function slopes $\frac{\partial\psi}{\partial y}$, as well as of the level slopes $\frac{\partial\zeta}{\partial y}$, are to be found in the north-western and south-eastern corners in agreement with solution (26), which arises from the combined effects of the Earth's rotation and bottom slopes (Figure 6). In this case the longitudinal current is the only southerly flow in the strait and has a velocity of about 20 cm/s. Its core is concentrated at the western boundary of the northern sill and at the eastern side of the southern limit of the strait.

The transverse circulation is negligible, reaching only a few cm/s at intermediate depths, and is of a two-layered type. The characteristic vertical movement consists of alternating upward and downward flows at both surface and lower levels. The strongest vertical currents (of order 10^{-2} cm/s) are also concentrated in the same south-easterly and north-westerly areas.

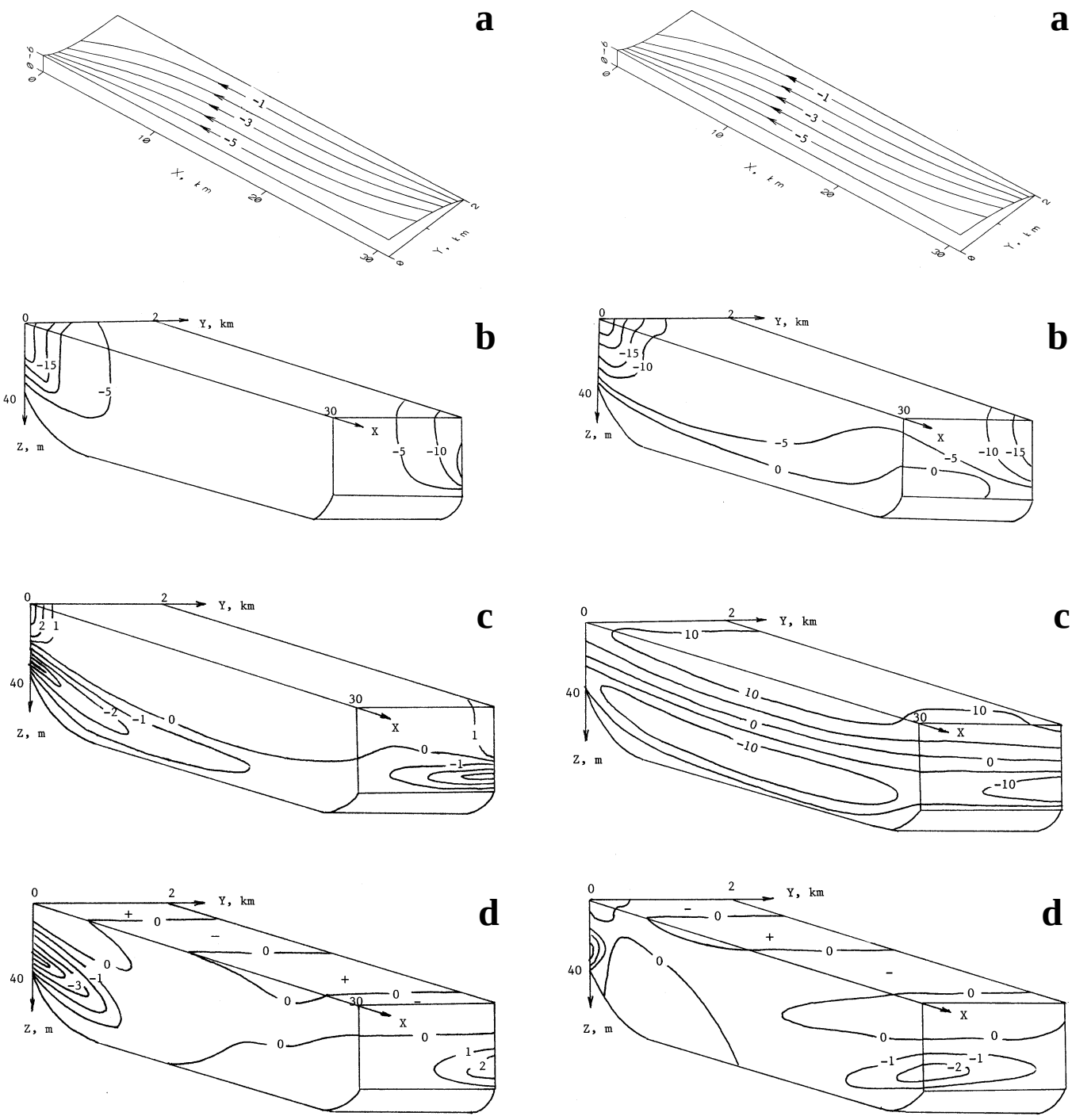

Fig.6. Distribution of the functions a) $\psi(x,y)\cdot 10^9$ cm^3/s, b) $u(x,y,z)$ cm/s, c) $v(x,y,z)$ cm/s, d) $w(x,y,z)\cdot 10^{-2}$ cm/s in experiment 1 (non-zero freshwater outflow, no wind, no density gradients).

Fig.7 Distribution of the functions a) $\psi(x,y)\cdot 10^9$ cm^3/s, b) $u(x,y,z)$ cm/s, c) $v(x,y,z)$ cm/s, d) $w(x,y,z)\cdot 10^{-2}$ cm/s in experiment 2 (like Figure 6, but non-zero density gradient in x direction).

The longitudinal density slope in the strait (Figure 7) suggests, when compared to the previous experiment, that there are insufficient variations in the stream line distribution $\psi(x,y)$. However, there are qualitative variations in the u-component of velocity, i.e. a two-layer current system is being formed. In this case a weak northward flow of the order of a few cm/s originates near the bottom. The undercurrent core is being formed at the eastern boundary of the northern sill and at the western side of the southern limit. The upper-layer current persists and is slightly intensified.

The v-component velocity structure preserves a two-layer character, and its intensity increases to 10 cm/s due to the addition of the baroclinic component to the transverse geostrophic balance. The typical characteristics of vertical motion in experiment 2 consist of a full replacement of the upwelling and downwelling areas, and a shift of the strongest currents to the north-eastern and south-western corners of the basin.

Taking into consideration the nonuniformity of the density field both along and across the strait (Figure 8) leads to the disappearance of the east-west current asymmetry as a result of the more uniform stream function slopes in comparison with experiment 2. The intensity of the longitudinal, cross-strait and vertical movements is however preserved.

An increase of the cross-strait density slope to $\rho_y = -10^{-9}$ cm^{-1} (experiment 4; Figure 9) results in a noticeable complication in depth-integrated circulation, and a general

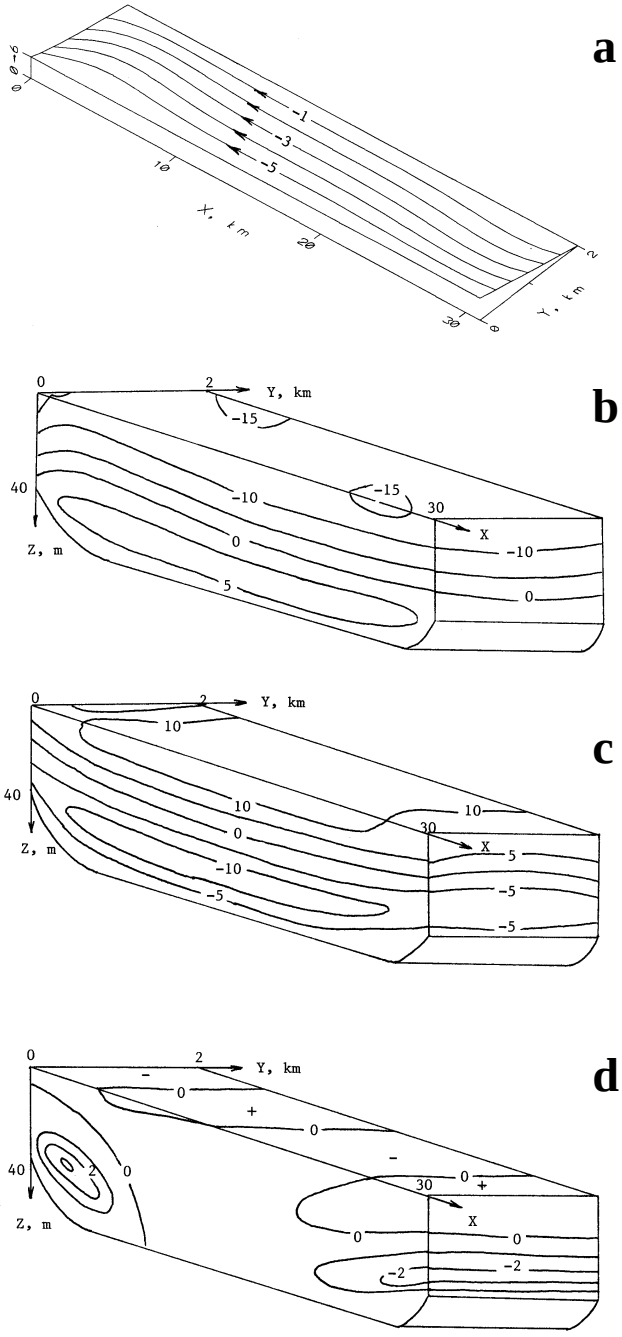

Fig. 8. Distribution of the functions a) $\psi(x,y) \cdot 10^9$ cm^3/s, b) $u(x,y,z)$ cm/s, c) $v(x,y,z)$ cm/s, d) $w(x,y,z) \cdot 10^{-2}$ cm/s in experiment 3 (like Figure 6, but non-zero density gradients in x and y directions).

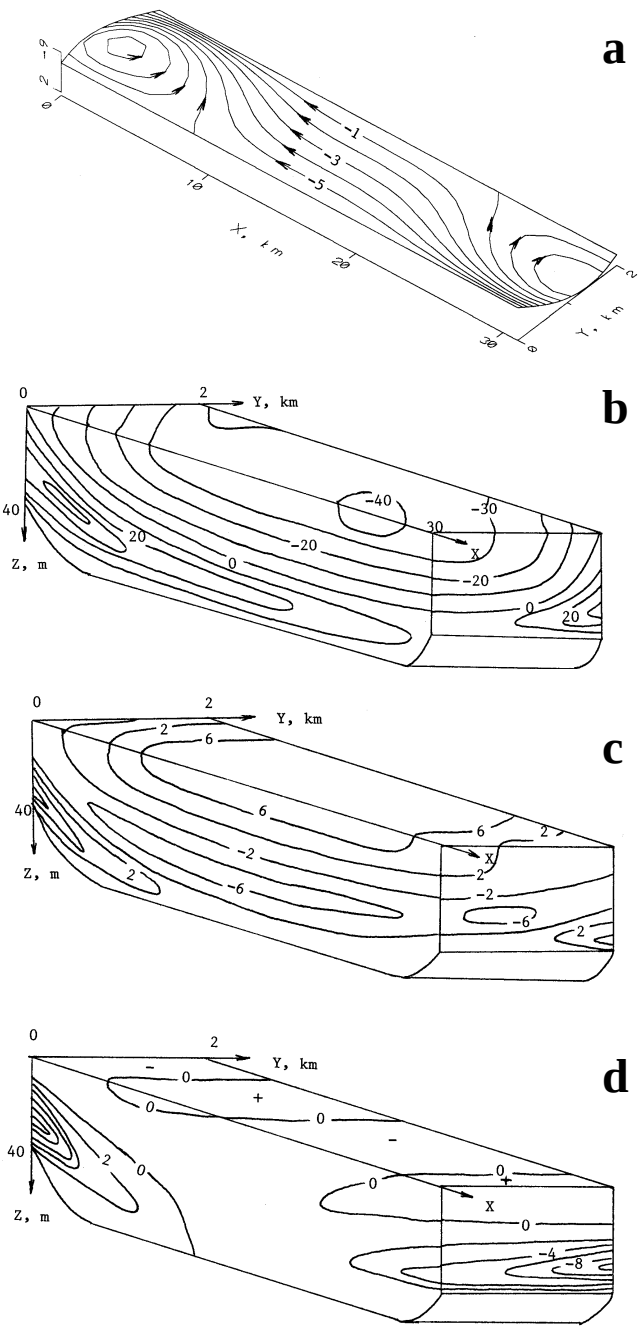

Fig. 9. Distribution of the functions a) $\psi(x,y) \cdot 10^9$ cm^3/s, b) $u(x,y,z)$ cm/s, c) $v(x,y,z)$ cm/s, d) $w(x,y,z) \cdot 10^{-2}$ cm/s in experiment 4 (like Figure 8, but greater density gradient in y direction).

increase in stream function gradients. The long-strait circulation is of a two-layer character, with the marked upper-layer and undercurrent flows having speeds of few tens of cm/s.

The transverse circulation decreases to a few cm/s, and should be of a three-layered character. Moreover, the positive values of the *u* and *v* underflow components may explain the observed north-westward spreading of Marmara Sea waters when flowing into the Black Sea. Oguz and Rozman (1991) alternatively suggest that such flow patterns may be associated with the presence of a submarine canyon.

The system of vertical movements maintains, as a whole, the same distribution of upwelling and downwelling zones as for the previous experiment, but with increased intensity. In this case, however, the maximum value of the *w*-component of velocity is shifted to the north-western and south-eastern corners of the channel. Among the experiments discussed here, these results are in closest agreement with the observed water dynamics of the Bosphorus strait.

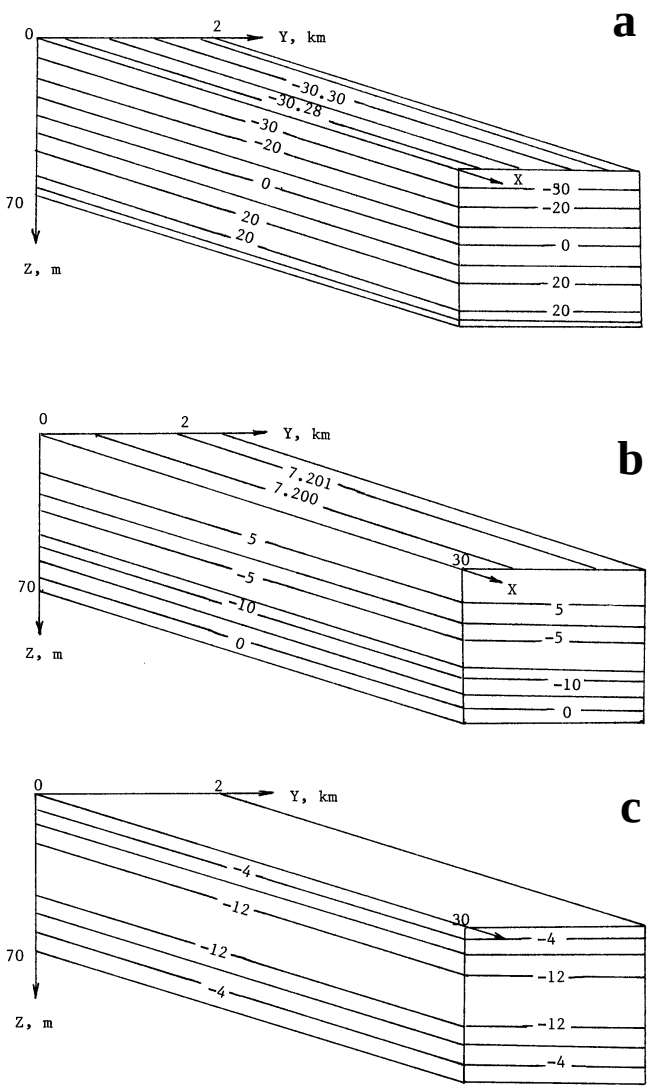

Fig.10. Distribution of the functions a) $u(x,y,z)$ cm/s, b) $v(x,y,z)$ cm/s, c) $w(x,y,z)\cdot 10^{-5}$ cm/s in experiment 5 (like Figure 9, but flat bottom).

The effect of differing parameter values on the kinematic structure can be briefly summarized as follows. In case of flat-bottomed straits (Figure 10), the current structure has an essentially linear character, indicating the importance of variable bottom topography in creating dynamical irregularities.

By contrast, the role of the β-effect is of no importance over the short length of the Bosphorus strait, because the western current intensification is very slight. The computation obtained by setting β=0 (Figure 11) virtually repeats the results of experiment 4; although a small difference arises due to a slight symmetrization of the $w(x,y,z)$ field in the region of weakest vertical flows. Because of the small β-effect, it is possible to simplify formulae (21) and (26).

Variations of the Ekman parameter, or of the coefficients of vertical turbulent exchange in experiments 7 and 8 (Figures 12 and 13, respectively) lead to a variation in Ekman layer thickness as compared to experiment 4, and a consequent general transformation of other dynamic features. Such variations also affect overall stream line distributions, the intensities of the currents, and the position of the interface between the upper and lower layer currents.

Possible changes in the kinematics of the strait, owing to a general decrease of fresh water inflow (due, for example, to run-off) were modelled in experiment 9. Assuming the adjoining sea to be a basin with zero fresh water budget (ψ_0=0) we find an intensification of the lower layer flow (Figure 14) when compared to experiment 4 (Figure 9).

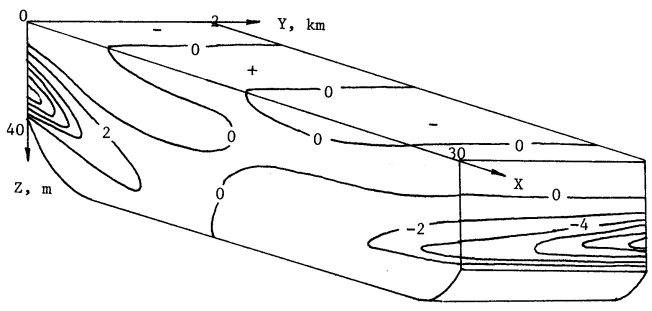

Fig. 11. Distribution of the function $w(x,y,z)\cdot 10^{-2}$ cm/s in experiment 6 (like Figure 9, but no β).

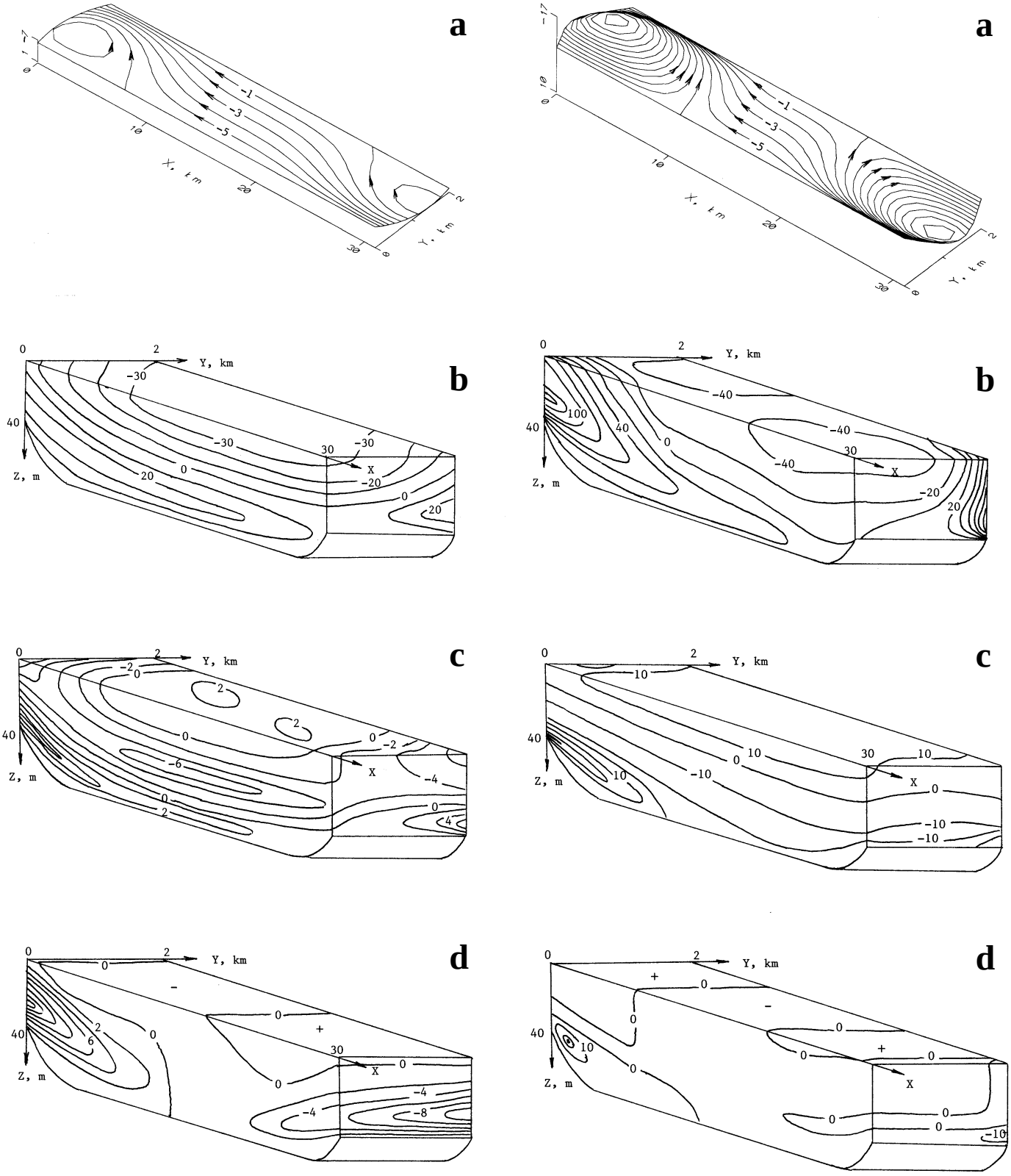

Fig. 12. Distribution of the functions a) $\psi(x,y) \cdot 10^9$ cm^3/s, b) $u(x,y,z)$ cm/s, c) $v(x,y,z)$ cm/s, d) $w(x,y,z) \cdot 10^{-2}$ cm/s in experiment 7 (like Figure 9, but smaller Ekman parameter).

Fig. 13. Distribution of the functions a) $\psi(x,y) \cdot 10^9$ cm^3/s, b) $u(x,y,z)$ cm/s, c) $v(x,y,z)$ cm/s, d) $w(x,y,z) \cdot 10^{-2}$ cm/s in experiment 8 (like Figure 9, but greater Ekman parameter).

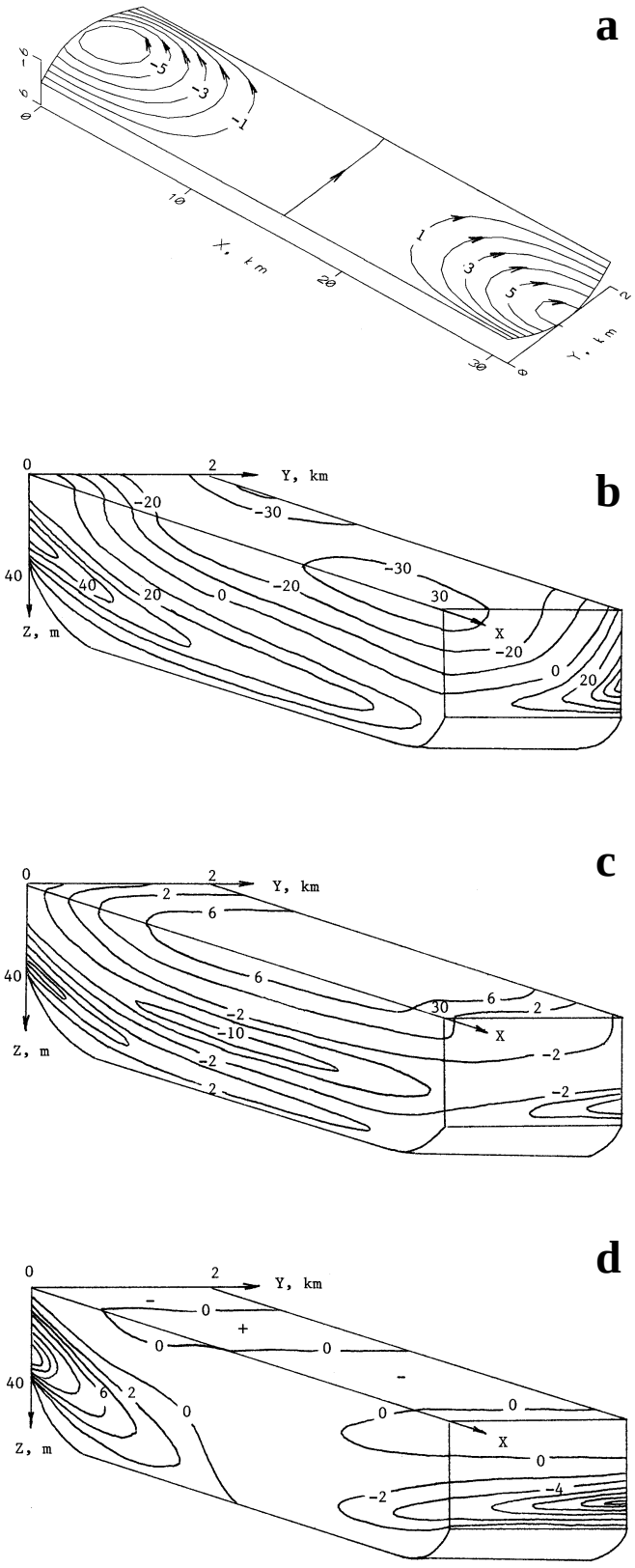

Fig. 14. Distribution of the functions a) $\psi(x,y) \cdot 10^9$ cm^3/s, b) $u(x,y,z)$ cm/s, c) $v(x,y,z)$ cm/s, d) $w(x,y,z) \cdot 10^{-2}$ cm/s in experiment 9 (like Figure 9, but no freshwater outflow).

Finally, wind is one of the most important regulating mechanism of water exchange through the strait. The intensity of wind-driven circulation forced by moderate winds (τ_x=-1) is of no importance, and does not exceed 10 cm/s (experiment 10; Figure 15). The influence of extremely strong winds with differing directions ($\tau_{x,y}$=±6.5) upon the dynamics of experiment 4 are presented in the last group of four experiments 11-14. Omitting a detailed description of the current field transformation, we find quantitative as well as qualitative changes of the kinematic water structure (Figures 16-19). In particular, a three-layered longitudinal circulation arises in the case of southern wind forcing, whilst an eastern wind causes blocking of the strait's undercurrent and noticeable changes in the intensity and character of transverse and vertical movements.

DISCUSSION AND CONCLUSIONS

We classify straits as: 1) long or short, 2) wide or narrow, 3) shallow or deep, 4) strongly or weakly stratified. This classification allows us to define the principal force terms in the momentum equations.

In the case of a long and strongly stratified strait, it is possible to neglect nonlinear acceleration and lateral exchange in comparison with vertical exchange and horizontal pressure gradients. The system of equations describing water circulation in such basins is a three-dimensional frictional model of Ekman type.

The density field was determined by the mean density surface slopes along and across the channel. Irregularities in bottom relief, including the presence of sills at the ends of the strait, were simulated by a parabolic shape for the bottom topography. For this problem, analytical solutions were also found using a Fourier method.

A frictional model of the Bosphorus strait yields a three-dimensional current structure, which is consistent with observations. The effect of external forcing upon the variability of the circulation was also analysed. We can provide an explanation for the formation of the two-layer current structure, and we estimate blocking conditions for the Bosphorus undercurrent. The model also enables us to explain the observed north-westward spreading of Marmara Sea waters entering the Black Sea.

The results confirm the importance of bottom slopes and the Earth's rotation in the development of the east-west current field asymmetry. Where the basin is narrow, the effect of the Earth's rotation seems to be negligible. It follows from Whitehead *et al.* (1974) that the parameter $\gamma_5 = \frac{D}{R}$, which

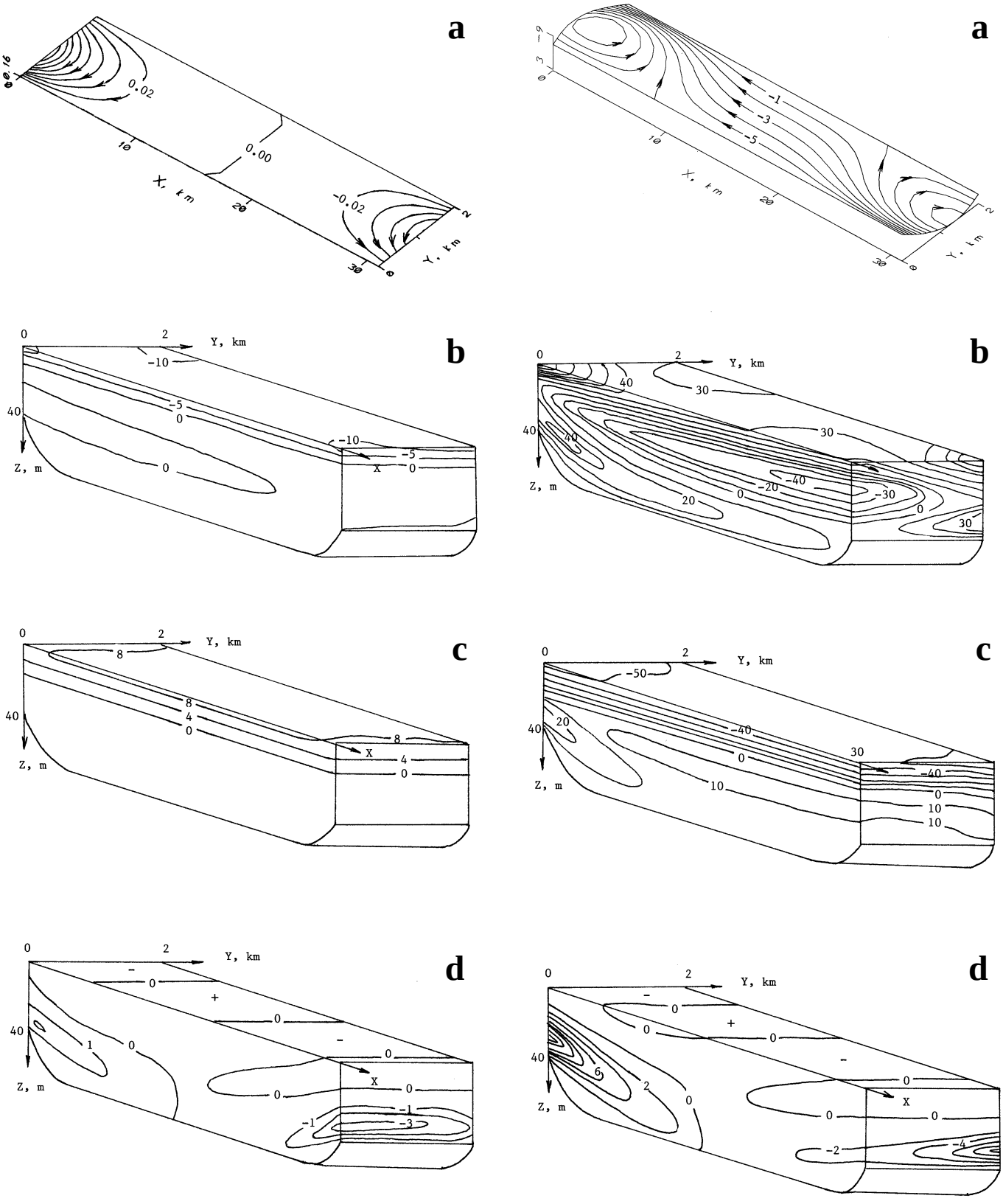

Fig. 15. Distribution of the functions a) $\psi(x,y) \cdot 10^9$ cm^3/s, b) $u(x,y,z)$ cm/s, c) $v(x,y,z)$ cm/s, d) $w(x,y,z) \cdot 10^{-3}$ cm/s in experiment 10 (moderate southward wind, no density gradients, no freshwater outflow).

Fig. 16. Distribution of the functions a) $\psi(x,y) \cdot 10^9$ cm^3/s, b) $u(x,y,z)$ cm/s, c) $v(x,y,z)$ cm/s, d) $w(x,y,z) \cdot 10^{-2}$ cm/s in experiment 11 (like Figure 9, but strong southern wind).

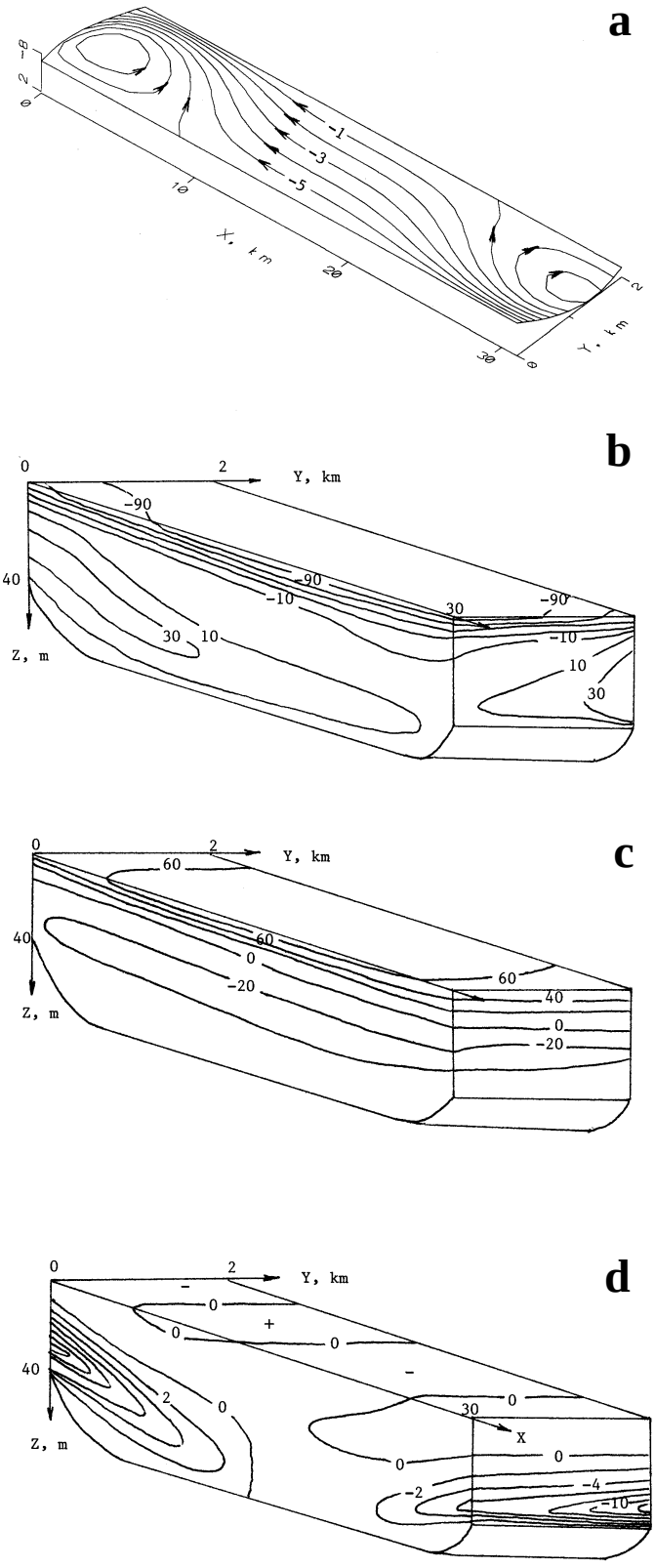

Fig. 17. Distribution of the functions a) $\psi(x,y) \cdot 10^9$ cm^3/s, b) $u(x,y,z)$ cm/s, c) $v(x,y,z)$ cm/s, d) $w(x,y,z) \cdot 10^{-2}$ cm/s in experiment 12 (like Figure 9, but strong northern wind).

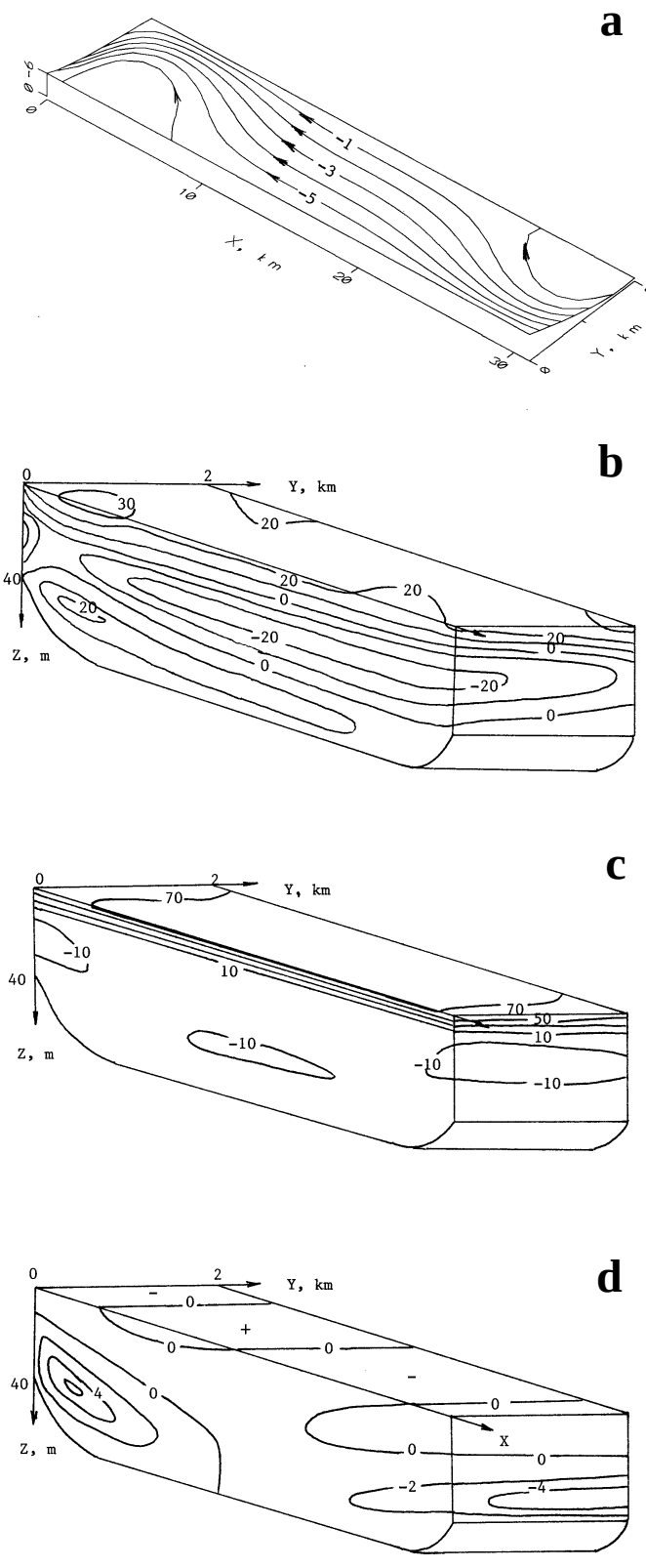

Fig. 18. Distribution of the functions a) $\psi(x,y) \cdot 10^9$ cm^3/s, b) $u(x,y,z)$ cm/s, c) $v(x,y,z)$ cm/s, d) $w(x,y,z) \cdot 10^{-2}$ cm/s in experiment 13 (like Figure 9, but strong easthern wind).

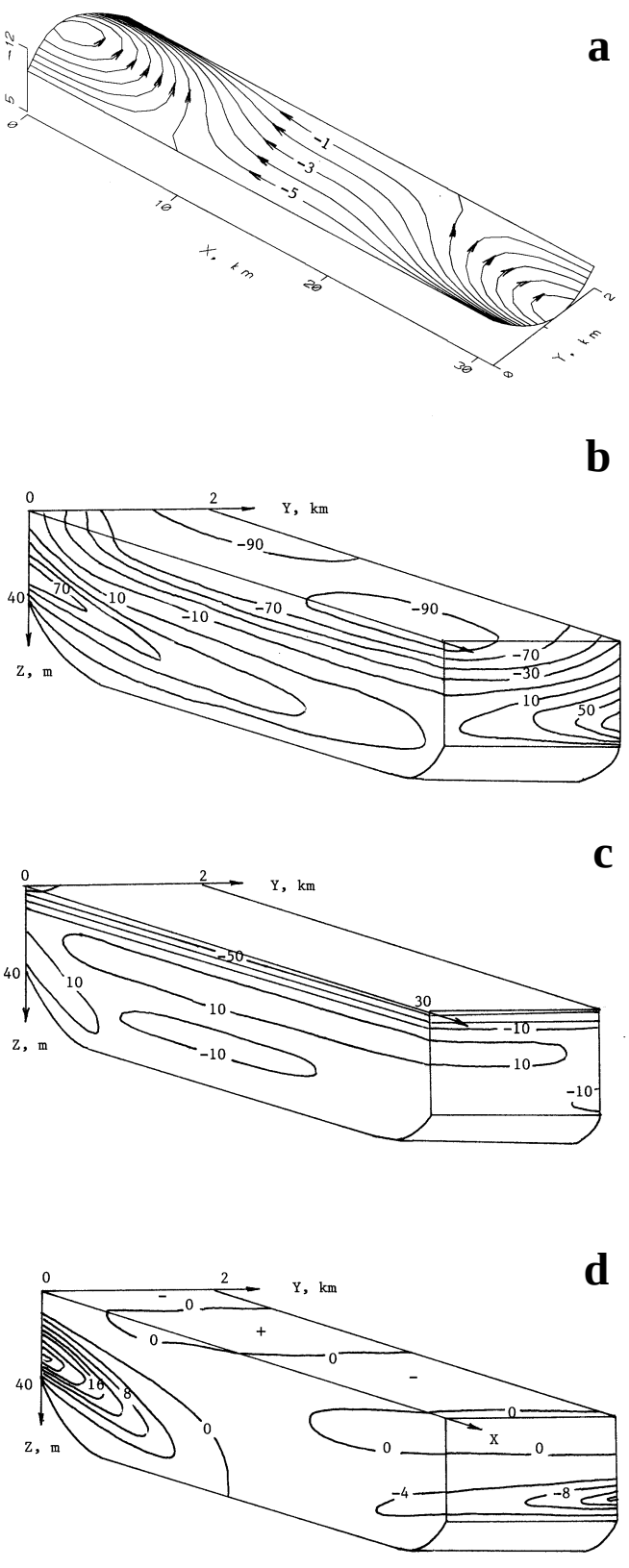

Fig. 19. Distribution of the functions a) $\psi(x,y) \cdot 10^9$ cm^3/s, b) $u(x,y,z)$ cm/s, c) $v(x,y,z)$ cm/s, d) $w(x,y,z) \cdot 10^{-2}$ cm/s in experiment 14 (like Figure 9, but strong westhern wind).

defines the ratio of Coriolis force to the horizontal pressure gradient, must be relatively small, and can probably be neglected in two-dimensional models. In the case of three-dimensional water circulation, however, it is important to include the Coriolis force.

The present frictional model supplements the present two-layer hydraulic control theory. The results of our dynamical theory for long straits may also be useful for interpreting circulation in other long and strongly stratified sea water bodies (bays, estuaries, seas) such as the Gulf of California, the Red Sea, the Adriatic Sea and others.

BIBLIOGRAPHY

ANATI, D.A., G. ASSAF and R.O.R.Y. THOMSON, 1977. Laboratory models of sea straits. *J. Fluid Mech., 81*, 341-351.

ARMI, L., 1986. The hydraulics of two flowing layers with different densities. *J. Fluid Mech., 163*, 27-58.

ARMI, L. and D. FARMER, 1985. The internal hydraulics of the Strait of Gibraltar and associated sills and narrows. *Oceanologica Acta, 8*, 37-46.

ASSAF, G. and A. HECHT, 1974. Sea straits: a dynamic model. *Deep Sea Res., 21*, 947-958.

BOGDANOVA, A.K. and V.N. STEPANOV, 1974. A hydrodynamic estimate of blocking conditions of the Bosphorus undercurrent. *Oceanology, 14, 1*, 48-52.

BRYDEN, H.L. and T.H. KINDER, 1991. Recent progress in strait dynamics. *Rev. Geophys. Suppl.*, 617-631.

BULGAKOV, S.N., 1991. Model of water exchange through the Bosphorus strait (a hydrodynamic estimate of blocking conditions for the Bosphorus undercurrent). *Sov. J. Phys. Ocean., 2, 3*, 171-178.

BULGAKOV, S.N., 1993. Peculiarities of the depth-integrated circulation in the straits. *Sov. J. Phys. Ocean., 4, 1*, 19-26.

BULGAKOV, S. N., G. K. KOROTAEV and J. A. WHITEHEAD, 1996a. The role of buoyancy fluxes in the formation of a large-scale circulation and stratification of sea water. Part 1: The theory. *Izvestiya - Atmospheric and Oceanic Physics, Engl. Transl., 32, 4*, 506-513.

BULGAKOV, S. N., G. K. KOROTAEV and J. A. WHITEHEAD, 1996b. The role of buoyancy fluxes in

the formation of a large-scale circulation and stratification of sea water. Part 2: Laboratory experiments. *Izvestiya - Atmospheric and Oceanic Physics, Engl. Transl., 32, 4*, 514-520.

BULGAKOV, S. N. and V. M. KUSHNIR, 1996. Vertical structure of the current field in the Northern Black Sea. *Oceanologica Acta, 19, 5*, 513-522.

CANDELA, J., 1991. The Gibraltar strait and its role in the dynamics of the Mediterranean Sea. *Dyn. Atmos. Oceans., 15*, 267-299.

EKMAN, V. M., 1932. Studien zur Dynamik der Meeresströmungen. *Gerlands Beitr. Geophysik, 36*, 385-438.

JOHNS, B. and T. OGUZ, 1990. The modelling of the flow of the water through the Bosphorus. *Dyn. Atmos. Oceans, 14, 3*, 229-258.

KINDER, T.H. and D.A. BURNS, 1986. A bibliography of the physical oceanography of straits. Naval Ocean Research and Development Activity Report 187 (available from Naval Oceans and Atmos. Research Laboratory, Stennis Space Center, MS, 39529-5004).

KINDER, T.H. and H.L. BRYDEN, 1990. Aspiration of deep water through the straits. *In:* The Physical Oceanography of Sea Straits. NATO ASI Ser., Kluwer Academic, Norwell, Mass. (edited by L.J. Pratt), 295-319.

MADERICH, V. S. and V. O. EFROIMSON, 1986. Simple model of the sea with the strait. *Oceanology, 31, 3*, 402-408.

MADERICH, V.S. and V.O. EFROIMSON, 1990. A contribution to the theory of the water exchange through the straits. *Oceanology, 30, 4*, 567-574.

MERZ, A., 1929. Hydrographische Beobachtungen in Bosphorus und Dardanellen. Veröff. Meereskunden, N.F., Berlin, 1.

OGUZ, T. and L. ROZMAN, 1991. Characteristics of the Mediterranean underflow in the south-western Black Sea continental shelf/slope region. *Oceanologica Acta, 14*, 5, 433-444.

OGUZ, T., E. OZSOY, M. A. LATIF, H. I. SUR and U. UNLUATA, 1990. Modelling of hydraulically controlled exchange flow in the Bosphorus Strait. *J. Phys. Ocean., 20*, 945-965.

SKIBA, Yu. N., 1989. Mathematical problems of the dynamics of viscous barotropic fluid on a rotating sphere. Department of Computational Mathematics, the USSR Academy of Sciences, Moscow, 1-178 (English transl.: Indian Inst. Tropical Meteorology, Pune, 1-211, 1990).

SUPPLEMENT TO ATLAS OF SEAS AND OCEANS (Terms. Notions. Reference tables), 1980. Izd. MO VMF USSR, 140 pp.

TOLMAZIN, D. M., 1967. Steady model of the water motion in stratified straits. *In:* Oceanographic Studies of the Black Sea. Kiev, Naukova Dumka, 18-34.

TOLMAZIN, D., 1985. Changing coastal oceanography of the Black Sea. *Progress in oceanography, 15*, 217-316.

UNLUATA, U., T. OGUZ, M. A. LATIF, and E. OZSOY, 1990. On the physical oceanography of the Turkish straits. *In:* The Physical Oceanography of Sea Straits. NATO ASI Ser., Kluwer Academic, Norwell, Mass. (edited by L.J. Pratt), 25-60.

WANG, D.-P., 1987. The strait surface outflow. *J. Geoph. Res., 92, 10*, 10807-10825.

WHITEHEAD, J.A., A. LEETMAA and R. A. KNOX, 1974. Rotating hydraulics of strait and sill flows. *Geophys. Fluid Dyn., 6*, 101-125.

S.N. Bulgakov and A. Martínez Zatarain
Instituto de Astronomía y Meteorología,
Universidad de Guadalajara,
Av. Vallarta 2602, 44130 Jalisco, México
E-mail: sbulgako@udgserv.cencar.udg.mx
Fax: (523) 615-9829